

1 **New biostratigraphic constraints show rapid emplacement of the Central Atlantic Magmatic**
2 **Province (CAMP) during the end-Triassic mass extinction interval**

3

4 Giulia Panfili^a, Simonetta Cirilli^a, Jacopo Dal Corso^b, Hervé Bertrand^c, Fida Medina^d, Nasrddine
5 Youbi^{e,f}, Andrea Marzoli^g

6

7 a) Dipartimento di Fisica e Geologia, Università degli Studi di Perugia, 06100-Perugia, Italy

8 b) School of Earth and Environment, University of Leeds, Leeds, West Yorkshire LS2 9JT, United
9 Kingdom

10 c) Laboratoire de Géologie de Lyon, Terre, Planètes, Environnement, UMR 5276 CNRS,
11 Observatoire de Lyon, Université et Ecole Normale Supérieure de Lyon 46 allée d'Italie, 69364
12 Lyon Cedex 07, France.

13 d) Moroccan Association of Geosciences, Rabat, Morocco

14 e) Geology Department, Faculty of Sciences Semlalia, Cadi Ayyad University, Prince Moulay
15 Abdellah Boulevard, P.O. Box 2390, Marrakech, Morocco.

16 f) Departamento de Geologia, Faculdade de Ciências and Instituto Dom Luís, Universidade de
17 Lisboa, Edifício C6, Campo Grande, 1749-016 Lisboa, Portugal

18 g) Dipartimento di Geoscienze, Università di Padova, 35131-Padova, Italy

19

20 **ABSTRACT**

21 Different lines of evidence suggest that the main trigger mechanism for the end-Triassic mass
22 extinction was the release of volcanic and thermogenic gases during the emplacement of the Central
23 Atlantic Magmatic Province (CAMP). However, the short duration of the biotic and environmental
24 crisis and the magmatic activity hinders precise control on the relative timing between these events,
25 especially when comparing the continental sedimentary record where there is no independent age
26 control with the magmatic record. In order to disentangle the temporal relationships of the end-

27 Triassic events, we have analyzed the palynology of the sedimentary strata interlayered with CAMP
28 lava flows from eleven sites throughout Morocco (Western and Central High Atlas, Middle Atlas,
29 Western Meseta). The recovered sporomorphs help to constrain the age of CAMP volcanism,
30 allowing the stratigraphic correlation of the basaltic volcanism with the extinction and geochemical
31 records such as carbon-isotope and mercury shifts, recorded in marine sedimentary successions
32 worldwide. Our new data show that CAMP erupted almost entirely during the end-Triassic mass
33 extinction interval, just before the Triassic–Jurassic boundary (Tr-J). Hence, a very rapid
34 emplacement of the CAMP very likely triggered the carbon cycle and ecological disruption at the
35 Tr-J boundary.

36
37 **Keywords:** *Central Atlantic magmatic province, end-Triassic mass extinction, Triassic-Jurassic*
38 *boundary.*

39

40 1. INTRODUCTION

41 The end of the Triassic, between about 201.7 and 201.3 Ma, (Schoene et al., 2010; Wotzlaw et al.,
42 2014; Davies et al., 2017) was characterized by three global events: 1) the emplacement of the
43 Central Atlantic magmatic province (CAMP) over 10 million square km in Europe, Africa, North
44 and South America (Marzoli et al., 1999, 2004, 2011; Blackburn et al., 2013; Davies et al., 2017);
45 2) the end-Triassic mass extinction, one of the big five mass extinctions of the Phanerozoic (Raup
46 and Sepkoski, 1982); 3) a severe perturbation of the carbon cycle as evidenced by three sharp
47 negative carbon isotope excursions (CIEs) in organic matter and marine carbonate, which are
48 recorded in several Tr–J stratigraphic sections (e.g. St Audries Bay, UK, Hesselbo et al. 2002;
49 Mariental, Germany, Heunisch et al., 2010; Stenlille, Denmark, Lindström et al., 2012). At the
50 GSSP Kuhjoch section, where the recorded excursions are only two, the first pronounced CIE has
51 been correlated with the *initial* CIE of St Audries Bay (Ruhl et al., 2009), marking the last

52 occurrence (LO) of the Triassic ammonite *Choristoceras marshi*. An older CIE (“Precursor CIE”),
53 preceding the “initial”, was described at St Audries Bay by Ruhl and Kürschner (2011).
54 The youngest long-term CIE (“Main CIE” sensu Hesselbo et al., 2002) starts shortly before the first
55 occurrence (FO) of the Jurassic ammonite species *Psiloceras planorbis*, marking the base of the
56 Jurassic (Hettangian). Due to the lack, in the UK record, of the ammonite species *Psiloceras*
57 *spelae*, chosen as biological marker for the base of the Jurassic (Hillebrandt et al., 2013), the
58 correlation with the GSSP section was based on the pollen taxon *Cerebropollenites thiergartii*,
59 recorded at Kuhjoch, approximately 3 m below the FO of the Jurassic ammonite (Kürschner et al.,
60 2007; Bonis et al., 2010; Hillebrandt et al., 2013).

61 Recently, Lindström et al. (2017) re-named the three end-Triassic to early Jurassic CIEs, in order of
62 time, as “*Marshi*”, “*Spelae*”, and “*Top Tilmanni*” on the base of biostratigraphic constraints.
63 Lindström et al. (2017) used as palynological marker the peak in abundance of *Polypodiisporites*
64 *polymicroforatus* considered more reliable than the FO of *C. thiergartii*, which seems not to be
65 synchronous in different areas (Heunisch et al., 2010; Lindström, 2016; Lindström et al., 2017).
66 In several north-western European localities such as St. Audrie's Bay (UK), Stenlille and Rødby
67 (Denmark), Mariental, Schandelah and Mingolsheim (Germany), Kuhjoch (Austria), the base of *P.*
68 *polymicroforatus* abundance is preceded by a negative CIE (Lindström et al., 2017). This CIE,
69 referred to as “*Marshi* CIE”, has been tentatively correlated with the negative C_{org}-excursion at the
70 top of the T-bed of the Kössen Formation at Kuhjoch (Lindström et al., 2017). The bed has been
71 associated with the LO of *C. marshi*, which marks the onset of the extinction (Hillebrandt et al.,
72 2013). The interpretation of Lindström et al. (2017) is in contrast with the traditional correlation
73 showing that the first CIE at Kuhjoch corresponds to the sharp *Initial* CIE at St Audries Bay
74 (Hesselbo et al., 2002, 2004; Ruhl et al., 2010; Hillebrandt et al., 2013), referred to as “*Main* CIE”
75 (second in time order) in Lindström et al. (2017). Geochronological data (zircon U/Pb ages;
76 Schoene et al., 2010, recalculated by Wotzlaw et al., 2014) and biostratigraphic correlations
77 (Lindström et al., 2017) suggest an age of about 201.51 ± 0.15 Ma for the *Marshi* CIE, shortly

78 preceding the *Spelae* CIE dated at about 201.39 ± 0.14 and the Tr–J boundary at 201.36 ± 0.17 Ma.
79 While the geochronologic and biostratigraphic data are now quite robust in defining the main end-
80 Triassic events, it remains problematic to define the relative timing of the CAMP and the ETE,
81 being both events clearly of very short duration, comparable to the errors of zircon U/Pb age data.
82 Moreover, the correlation of CAMP magmatism (a continental event) with the ETE and the
83 negative CIEs (mostly recorded and solidly age-constrained in marine sequences) is very
84 problematic (e.g. Dal Corso et al., 2014; Lindström et al., 2017). While CAMP intrusions are now
85 well dated (201.63 ± 0.03 to 200.92 ± 0.06 Ma; Blackburn et al., 2013; Davies et al., 2017),
86 available geochronologic data for the volcanic rocks are much less precise. Recent studies show an
87 increase in mercury concentrations within the interval between the beginning of the ETE and the
88 Tr–J boundary, further supporting the hypothesis that CAMP emplaced in a very short time
89 (Thibodeau et al., 2016; Percival et al., 2017). However, the exact role of CAMP volcanism in
90 triggering the CIEs and the ETE remains questionable. The end-Triassic negative CIEs suggest a
91 massive input into the atmosphere of large quantities of ^{13}C -depleted CO_2 (Hesselbo et al., 2002;
92 Ruhl et al., 2011; Dal Corso et al., 2014). Given the synchrony, the emplacement of CAMP is the
93 most likely trigger of the negative CIEs (Marzoli et al., 2004; Guex et al., 2004; Bonis et al., 2010;
94 Whiteside et al., 2010; Ruhl et al., 2011), via repeated magmatically triggered releases of highly
95 depleted thermogenic CO_2 and CH_4 and/or clathrate methane (Dickens et al., 1995; Svensen et al.,
96 2004; Davies et al., 2017). The emission of volcanogenic gases such as CO_2 or SO_2 (Callegaro et
97 al., 2014) could be invoked as the initial trigger of the ETE. Notably, increase of atmospheric $p\text{CO}_2$
98 recorded by fossil leaf stomata and soil carbonates has been predicted to cause global warming and
99 ocean acidification during the time of peak CAMP magmatic activity (McElwain et al., 1999; Bonis
100 et al., 2010; Schaller et al., 2011; Martindale et al., 2012). The continental volcano-sedimentary
101 sequences of North America and Morocco record a negative CIE in the bulk organic matter and
102 Late Triassic sporomorph assemblages below the first known CAMP basalt (Whiteside et al., 2010;
103 Deenen et al., 2010, 2011; Dal Corso et al., 2014). It remains controversial, to which of Rhaetian

104 CIEs this continental CIE can be correlated. Based on an extensive review of the published
105 literature and new data from Denmark and Germany, by combining biostratigraphic, geochemical
106 and geochronological constraints, Lindström et al. (2017) argued that most of CAMP basalts were
107 emplaced in correspondence to the *Marshi* CIE and before the *Spelae* CIE. Hence, nearly the entire
108 sequence of CAMP basalts in Morocco could have been erupted before and/or during the ETE
109 interval. To test this hypothesis, we studied the palynological association of the sedimentary strata
110 interlayered within the volcanic sequences in the Argana valley (Western High Atlas), the Central
111 High Atlas, the Middle Atlas, and the Western Meseta, from the base of the CAMP basaltic flows to
112 the top of the lava pile, with the aim to biostratigraphically constrain the age of the volcano-
113 sedimentary sequence of Morocco and thus the duration of CAMP volcanism.

114

115 **2. GEOLOGICAL SETTING**

116 CAMP lava flow sequences crop out in several areas of central and northern Morocco, i.e. in the
117 Central High Atlas (CHA), the Western High Atlas (Argana valley), the Middle Atlas, the Eastern
118 and the Western Meseta (Fig. 1). These volcanic sequences reach a maximum thickness of nearly
119 300 m in the southern CHA, while in the northern CHA, the Argana valley and the Middle Atlas,
120 the maximum preserved thickness of basaltic flows reaches some 150 m. The lava flows have been
121 subdivided into four main informal units based on geochemical, volcanological, and
122 magnetostratigraphic data (Bertrand et al., 1982; Knight et al., 2004; Marzoli et al., 2004; El
123 Hachimi et al., 2011). These units are named Lower, Intermediate, Upper and Recurrent Basalt.
124 Lower and Intermediate Basalt are present in (almost) all lava flow sequences and constitute about
125 90% of the preserved volume of effusive CAMP rocks in Morocco (Fig. 2). The Lower Basalt is
126 missing only in the northwestern Middle Atlas (as for example near the village of Agourai; Fig. 1),
127 where the stratigraphically lowest basaltic lava flows have geochemical compositions pertaining to
128 the Intermediate Basalt. The Upper Basalt is widespread in the CHA and occur sporadically in the
129 Middle Atlas (e.g., at Midelt or at Tounfite section), while they are absent in the Argana Valley.

130 Recurrent Basalt are limited to the CHA and volumetrically negligible with respect to the rest of the
131 lava piles (Marzoli et al., 2004). Over 20 high quality $^{40}\text{Ar}/^{39}\text{Ar}$ ages are available for the Moroccan
132 CAMP (Knight et al., 2004; Nomade et al., 2007; Verati et al., 2007; Marzoli et al., 2011). These
133 data indicate that the Lower to Upper Basalt were erupted at approximately 201.5 Ma, in a time-
134 span shorter than the analytical uncertainties of the $^{40}\text{Ar}/^{39}\text{Ar}$ ages (roughly 0.5-1.5 Ma). One
135 intrusive rock from the Argana basin (the Amelal sill) yielded a U/Pb zircon age of 201.56 ± 0.05
136 Ma and was assigned to the Intermediate Basalt (Blackburn et al., 2013). Only the Recurrent Basalt
137 yielded significantly younger $^{40}\text{Ar}/^{39}\text{Ar}$ ages (approximately 199 Ma; Verati et al., 2007).
138 Magnetostratigraphic data support a (very) short duration of eruption of Lower to Upper Basalt,
139 since these were erupted as a total of five very short-lived volcanic pulses, each probably lasting
140 just a few centuries (Knight et al., 2004).

141 The first CAMP basaltic lava flows were emplaced throughout Morocco on fine-grained silty
142 deposits of probably lacustrine or lagoonal origin. Presence of load casts and a generally
143 conformable layering of the sedimentary strata beneath the first lava flows indicates that lavas
144 flowed over still soft sediments, arguing against a significant sedimentary gap before emplacement
145 of the first CAMP lavas. These Lower Basalt flows emplaced subaerially (El Hachimi et al., 2011).
146 Evidence for a progressive subsidence of the basins during emplacement of the basalts comes from
147 widespread pillow lava structures observed at the base of the Intermediate lava formation (El
148 Hachimi et al., 2011), and changes in detrital zircon source into the CHA and Argana basins
149 (Marzoli et al., 2017). The thin columnar jointing of the Upper Basalt suggests that also these flows
150 were emplaced under water. Sedimentary strata between the Intermediate and the Upper, and then
151 on top of the Upper Basalt include carbonate layers, testifying for a further subsidence. This
152 progressive ongoing subsidence argues against significant sedimentation gaps after emplacement of
153 each flow package.

154

155 **3. SAMPLED SECTIONS AND METHODS**

156 For the palynological analysis we sampled intra- and infra-basaltic sediments from localities in the
157 Argana valley (Western High Atlas; 2 sites), the Central High Atlas (CHA; 4 sites), the Middle
158 Atlas (4 sites), and the Western Meseta (1 site) (Figs. 1; 2). All productive samples (except three,
159 AN69, AN64 and AN520) were collected at the base of the CAMP lava piles, at stratigraphic
160 distances of about 1 meter to about 5 cm below the first preserved Lower Basalt. Three sampling
161 localities from the CHA provided productive samples at the base of the Lower Basalt flows, namely
162 at Tiourjdal (southern CHA) and at Oued Lahr and Oued Amassine (Northern CHA). Samples from
163 two of the studied localities (Tiourjdal and Oued Lahr) were already investigated by Marzoli et al.
164 (2004), but were reprocessed and reanalyzed for our new study. In the northern CHA (Oued Lahr
165 and Ikourker localities), also sedimentary layers located between the Upper and the Recurrent
166 Basalt resulted productive (samples AN69, AN64). Middle Atlas sampling sites included two
167 sections, one near the village of Teklit (Tounfite section, near the Oum-Rbia river sources), and one
168 near Agourai. For this latter the productive sample is located at the base of the Intermediate Basalt.
169 Two sections (Ahouli and Ajoundou N'fnouss) were sampled near Midelt, located at the
170 intersection between the CHA and the Middle Atlas in central Morocco. Furthermore, we collected
171 productive sediments at the base of the Maaziz sequence, in the Western Meseta (northwestern
172 Morocco). The whole set of samples including also the non-productive ones are reported in the
173 online supplementary Table 1 along with lithological description, stratigraphic position and
174 geographic coordinates. The palynological preparations were made at the Sedimentary Organic
175 Matter Laboratory of the Department of Physics and Geology, University of Perugia (Italy).
176 Samples were crushed and then processed using a standard technique for palynological analysis
177 (Green, 2001; Wood et al., 2002). Details on methods are reported in the online supplementary
178 material.

179

180 **4. RESULTS**

181 The occurrences of the sporomorphs detected in the analyzed samples are given in Fig. 2 and the
182 full species list and the results of the quantitative analysis in the online supplementary Table 2,
183 Table 3 and Fig. S1. The main palynological markers are illustrated in Fig.3. In the Argana basin,
184 all the samples from the strata below the Lower Basalt were productive and yielded a palynological
185 assemblage, which includes abundant *Classopollis* group (*Classopollis meyerianus*, *Classopollis*
186 *murphyae*, *Classopollis torosus*) and common *Patinasporites densus* in association with rare to
187 common *Calamospora mesozoica*, *Ricciisporites tuberculatus*, *Todisporites* sp., *Triadispora* sp. and
188 *Tsugaepollenites pseudomassulae*.

189 In the CHA basin (southern Tiourjidal section and northern Oued Lahr, Oued Amassine, and
190 Ikourker sections), the palynological assemblage detected in all strata at the base of the Lower
191 Basalt is similar to that of the Argana basin. In the southern CHA section of Tiourjidal (samples
192 AN50, AN52 and AN150), the association is dominated by *Classopollis* group of which common *C.*
193 *meyerianus*, common to abundant *C. murphyae* and common *C. torosus*. Variable percentages of *P.*
194 *densus* (from rare to abundant), rare *C. mesozoica*, *Perinopollenites elatoides*, *Parvisaccites*
195 *triassicus*, *Vitreisporites pallidus* and bisaccate pollen (e.g. *Alisporites* sp., *Triadispora* sp.) also
196 occur. The assemblage recorded in the northern CHA sections of Oued Lahr (samples AN59,
197 AN60) and Oued Amassine (AN1 sample) yielded rare to abundant *Classopollis* spp. (with higher
198 percentages of *C. meyerianus*) and common *P. densus*, in association with common *C. mesozoica*,
199 rare *R. tuberculatus*, *T. pseudomassulae*, *Alisporites* sp. and *Triadispora* sp.. In the Middle Atlas
200 (Tounfite, sample AN533) and Midelt sections (Ahouli, sample AN214 and AN221), the
201 sedimentary beds at the base of the Lower Basalt yielded a microfloral assemblage containing
202 abundant *C. meyerianus* and rare to common *C. torosus* in association with common *P. densus*, and
203 rare *Enzonasporites vigens*, *Ovalipollis ovalis*, *Ovalipollis pseudoalatus*, *Vallasporites ignacii*
204 and *Vesicaspora fuscus*. The base of the Maaziz sequence (Western Meseta, sample AN 600) below
205 the Lower Basalt yielded a palynological association comparable with that of the Tiourjidal section
206 (CHA) marked by the abundance of *C. meyerianus* in association with frequent *P. densus* and rare

207 *C. torosus* and bisaccate pollen such as *Alisporites similis* and *Alisporites* sp.. ~~Productive samples~~
208 ~~are available~~ Also the sedimentary layers at the base of the Intermediate and above the Upper Basalt
209 flows in the sections of the CHA and Middle Atlas basins result to be palynologically productive.
210 The sedimentary interval at the base of the Agourai basaltic flows (Middle Atlas basin, sample
211 AN520) yielded an assemblage with abundant *C. meyerianus* and rare *C. torosus* in association with
212 common *P. densus*. Notably, here the lowest flows pertain to the Intermediate Basalt, which are
213 conformably emplaced on top of the analyzed siltstone layer. At the Oued Lahr and Ikourker
214 sections (northern CHA) the palynological assemblage of the samples AN69, AN203 and AN64
215 from the sedimentary strata between the Upper and the Recurrent Basalt is still characterized by the
216 dominance of the *Classopollis* group (abundant *C. meyerianus* and *C. murphyae* and common *C.*
217 *torosus*) and rare to common *P. densus*, in association with rare long range species such as
218 *Alisporites* sp. and *C. mesozoica*.

219

220 5. DISCUSSION

221 5.1 Biostratigraphic constraints on CAMP volcanism

222 The palynoassemblages characterizing the sedimentary layers below the first flow in the CHA and
223 Argana basins, below the Intermediate flows in the Middle Atlas (at the Agourai section), and
224 above the Upper Basalt flows in the CHA can be overall ascribed to the Rhaetian. The dominance
225 of *Classopollis* spp. and the presence of taxa typical of Late Triassic assemblages, such as common
226 *Patinasporites densus* and rare *Enzonalasporites vigens*, *Tsugaepollenites pseudomassulae* and
227 *Vallasporites ignacii* confirm this hypothesis.

228 The Last Occurrence Datum (LOD) of *P. densus*, was commonly recorded and well documented in
229 marine sedimentary successions, before the end of the Rhaetian (Cirilli, 2010; Kürschner and
230 Hengreen, 2010). In continental settings (e.g. Chinle Formation, Colorado Plateau), *P. densus* was
231 recorded in Norian – early Rhaetian sedimentary strata (Litwin et al., 1991; Irmis et al., 2015)
232 together with *Enzonalasporites* and *Vallasporites*) (Lindström et al., 2016). In some Moroccan

233 samples (Ahouli and Midelt section), rare specimens of *E. vigens* and *V. ignacii* are recorded in co-
234 occurrence with *P. densus*, in association with the dominant *Classopollis* group therefore
235 suggesting an age slightly older than latest Rhaetian (Cirilli et al., 2010; Lindström et al., 2016).
236 The Late Triassic age is further confirmed by the absence of Jurassic palynological diagnostic
237 markers such as *Cerebropollenites thiergartii* and/or the acme of *Polypodiisporites*
238 *polymicroforatus* (Hillebrandt et al., 2013; Lindström et al. 2017).

239 The Moroccan palynological associations dominated by the *Classopollis* group in association with
240 *P. densus*, coming from the sedimentary layers intercalated with the Intermediate and Upper Basalt,
241 are very similar to those recorded in the continental sedimentary successions of Fundy (Nova
242 Scotia, Fowell and Traverse, 1995; Cirilli et al., 2009) and Newark basins (eastern North America
243 (Whiteside et al., 2010 and references cited therein). Both in the Fundy basin and in the Newark
244 basin, the highest record of *P. densus* occurs below the oldest CAMP lava flow, whilst, in Morocco,
245 it does not disappear before the first CAMP basalt. It is still recorded at the base of the Intermediate
246 lava flows, as well as above the Upper Basalt of Morocco, permitting to date as Late Triassic the
247 entire sedimentary sequence. The presence of *E. vigens* and *V. ignacii* in the sedimentary
248 intercalations at the base of Lower Basalt in the Ahouli and Midelt section let to consider a slightly
249 earlier onset of CAMP volcanism in Morocco than in the Newark basin, USA. This has already
250 been suggested by Marzoli et al. (2004) based on geochemical, magnetostratigraphic, and
251 biostratigraphic data and seems consistent also with recent geochronological data (Blackburn et al.,
252 2013). Therefore, the palynological data from the entire CAMP sedimentary sequence in Morocco
253 could suggest a diachronous emplacement of lava flows. The age attribution of the Moroccan
254 CAMP flows to the latest Triassic has further implications for the correlation of the CAMP activity
255 to end-Triassic CIEs and mass extinction. Deenen et al. (2010) and Dal Corso et al. (2014) found a
256 negative CIE below the Lower Basalt of the Argana valley and of the CHA (Fig. 4). Dal Corso et al.
257 (2014) suggested that this negative CIE was likely caused by eruption of early CAMP lava flows
258 that have been rapidly eroded after their emplacement (see also Schaller et al., 2011), as witnessed

259 by the chemical and mineralogical composition of the infra-basaltic sediments. Additionally, early-
260 emplaced CAMP intrusions could have triggered the release of depleted thermogenic CO₂ or CH₄,
261 thus causing the carbon-cycle disruption CIE (Davies et al., 2017). Magnetostratigraphic and
262 chemostratigraphic data have been used to correlate the negative CIE below the Lower Basalt unit
263 in Morocco with the “*initial*” CIE recorded at St. Audries Bay and GSSP (Kuhjoch) sections
264 (Kürschner et al., 2007; Bonis et al., 2010; Deenen et al., 2010; Hillebrandt et al., 2013; Dal Corso
265 et al., 2014). Considering the correlation proposed by Lindström et al., (2017), the infra-basaltic
266 negative CIE in Morocco could be alternatively correlated to the *Marshi* CIE (Fig. 4). The
267 correlation between the Moroccan assemblages and those found in the key marine sections for the
268 Tr-J boundary (e.g. Kuhjoch, Hillebrandt et al., 2013; St. Audries Bay, Bonis et al., 2010) results to
269 be difficult because of the several dissimilarities among the assemblages and the lack of ammonite
270 stratigraphy in the Moroccan successions, which are deposited in continental to coastal
271 environments. Nevertheless, at least the sedimentary levels below the Lower Basalts, containing
272 common *P. densus* in association with *E. vigens* and *V. ignacii*, and the last co-occurrences of *O.*
273 *ovalis*, *T. pseudomassulae*, and *R. tuberculatus* could be correlated with the the *Rhaetipollis* –
274 *Limbosporites* (RL) palynozone of the GSSP for the Tr–J boundary at Kuhjoch (Fig. 4), and to the
275 Rhaetian assemblage SAB1 defined for the marine Tr–J boundary section at St. Audries Bay in the
276 UK (Bonis et al., 2010) (Fig. 4). The absence of other, more specific palynozone markers in our
277 samples hampers a higher resolution and a more detailed correlation between the European sections
278 and the sedimentary layers intercalated with the Intermediate and Upper Basalt. However, the
279 palynological assemblages justify the age attribution of the entire sedimentary sequence in Morocco
280 to the Rhaetian and therefore below the higher portion of the TH and SAB 4 zones, including the
281 Tr-J boundary, from Kuhjoch and St. Audries Bay, respectively.

282 Combining the carbon isotopic data (Deenen et al., 2010; Dal Corso et al., 2014) and the new
283 palynological data, the emplacement of (almost) the entire volcanic pile of CAMP in Morocco
284 occurred within the ETE interval (Fig. 4). The onset of CAMP volcanism in Morocco, shortly

285 preceded by a negative CIE may be either correlated to the precursor (*Marshi* sensu Lindström et
286 al., 2017) or to the initial (*Spelae* sensu Lindström et al., 2017) CIE at St. Audries Bay. In either
287 case, our data constrain the short duration of CAMP volcanism in Morocco, which occurred entirely
288 within the ETE interval. Within this interval, high mercury concentrations have been recorded in
289 several sedimentary successions, including St. Audries Bay and Kuhjoch (Fig. 4) and have been
290 interpreted as the signal of large-scale emissions of volcanic gasses from CAMP (Thibodeau et al.,
291 2016; Percival et al., 2017). Our study confirms this hypothesis.

292

293 **5.2 Implications for the duration of CAMP volcanism**

294 The Moroccan palynological assemblages, integrated with the carbon isotope data, constrains nearly
295 the entire sequence of CAMP basalts in Morocco within the Rhaetian and thus during the ETE
296 interval. Deenen et al. (2010) estimated that the CAMP volcanism can be linked to the onset of two
297 pulses of flood basalts. The first pulse (Moroccan event) can be linked to the initial CIE. The
298 second pulse (just 20 Kyrns apart from the first one) pre-dates the Tr–J boundary by about 80 Kyrns,
299 resulting in a very brief duration of the CAMP volcanism of less than 100 Kyrns. Based on the U/Pb
300 ages obtained from the Rhaetian–Hettangian sequences of the Pucara basin in Peru, the ETE
301 interval had an estimated duration of about 150 Kyrns (from 201.51 ± 0.15 Ma to 201.36 ± 0.17 Ma;
302 Schoene et al., 2010; Wotzlaw et al., 2014). Using carbon isotope data from marine carbonates from
303 Peru and assuming a constant sedimentation rate, Yager et al. (2017) estimated a slightly longer
304 duration of this interval (0.28 ± 0.09 Ma). This implies that 95% of CAMP volcanism in Morocco
305 was erupted in less than 150 Kyrns (or less than 280 Kyrns, following Yager et al., 2017). This is
306 consistent with the U/Pb age obtained by Blackburn et al. (2013) for the Amelal sill (201.56 ± 0.05
307 Ma). More recently, the correlations of Lindström et al. (2017) highlighted that both the lower and
308 intermediate CAMP basalts are synchronous to or pre-date the *Marshi* CIE and the extinction
309 interval. Very rapid emplacement of CAMP basaltic flows is also consistent with previous
310 magnetostratigraphic studies of the Tiourjidal volcanic pile (Knight et al., 2004) that showed that

311 basaltic eruptions occurred as a series of five pulses, each of which lasted less than a secular
312 variation cycle (about 450 years by analogy with the duration of these cycles in the Holocene;
313 Schnepp et al., 2003). Summarizing, our new findings and the previous geochronologic and
314 magnetostratigraphic data indicate that the emplacement of the CAMP was a very rapid event,
315 which occurred during the ETE interval.

316

317 **6. CONCLUSIONS**

318 New palynological data from the volcano-sedimentary sequences of the Central High Atlas, Middle
319 Atlas and Argana basins in Morocco constrain the age of CAMP volcanism in Morocco to the latest
320 Triassic (Rhaetian). The occurrence of palynological assemblages characterized by the *Classopollis*
321 group in association with the index Triassic species *Patinasporites densus* from the sedimentary
322 strata below the Lower and Intermediate Basalt to those above the Upper Basalt allows assigning
323 almost the entire CAMP volcanism (Lower, Intermediate, and Upper flows) to the Rhaetian. The
324 occurrence in some Moroccan samples (Ahouli and Midelt sections) collected below the Lower
325 Basalt of rare specimens of *Enzonalasporites vigens* and *Vallasporites ignacii* suggests an age
326 slightly older than latest Rhaetian and in turn an earlier emplacement of the CAMP in Morocco than
327 in the North America (Newark and Fundy basins). The palynological data let to tentatively correlate
328 the sedimentary strata below the Lower Basalt to the older Rhaetian palynozones defined in the
329 Kuhjoch sections (*Rhaetipollis* – *Limbosporites* (RL), and in the St. Audries Bay (SAB1). Although
330 the lack of palynological markers prevent a detailed correlation, the palynological assemblages
331 from the sedimentary beds intercalated with the Intermediate and the Upper Basalt indicate a
332 Rhaetian age and constrain the CAMP basalt eruption below the higher portion of the TH and SAB
333 3 zones from Kuhjoch and St. Audries Bay respectively.

334 Beyond the still debated possible correlations that can be adopted to correlate marine Tr–J section
335 (e.g., the GSSP at Kuhjoch and St. Audries Bay), the associations recovered in the sedimentary
336 strata, both below and above the Moroccan CAMP basalt flows, are Rhaetian, thus excluding an

337 early Jurassic age for the volcanic pile. By combining the carbon isotopic data and U-Pb ages with
338 the new palynological data, we show that the emplacement of almost all CAMP basalts in Morocco
339 occurred during the end-Triassic extinction interval and was very fast (probably less than 150
340 Kyr). Hence, our results precisely link the ETE to the CAMP volcanism. This shows that very
341 rapid release of large amounts of volcanic gases (mainly CO₂ and SO₂) into the latest Triassic
342 atmosphere – land – ocean system caused widespread disruption of the ecosystems.

343

344 **ACKNOWLEDGMENTS**

345 The paper greatly benefits of the revision of Sofie Lindström (Geological Survey of Denmark and
346 Greenland, Copenhagen, Denmark) and of an anonymous reviewer.

347 This study was partly supported by funds of the Sedimentary Organic Matter Laboratory of the
348 Department of Physics and Geology (Perugia University), Grant number: CONLABSSOR-000934 -
349 SC and by PhD funds (GP). The authors (NY, JDC, AM) are grateful to CNR-Italy, CNRST
350 Morocco for financial support of fieldwork. JDC acknowledges the Hanse-Wissenschaftskolleg
351 (Delmenhorst, Germany) for the financial support.

352

353 **REFERENCES**

354 Bertrand, H., Dostal, J., Dupuy, C., 1982. Geochemistry of early Mesozoic tholeiites from Morocco.

355 Earth and Planetary Science Letters, 58, 225–239. DOI: 10.1016/0012-821X(82)90196-0

356 Blackburn, T.J., Olsen, P.E., Bowring, S.A., McLean, N.M., Kent, D.V., Puffer, J., McHone, G.,

357 Rasbury, E.T., Et-Touhami, M., 2013. Zircon U-Pb Geochronology Links the End-Triassic

358 Extinction with the Central Atlantic Magmatic Province. Science, 340, 941-945.

359 DOI:10.1126/science.1234204

360 Bonis, N.R., Ruhl, M., Kürschner, W.M., 2010. Milankovitch-scale palynological turnover across

361 the Triassic-Jurassic transition at St. Audrie's Bay, SW UK. Journal of the Geological Society

362 of London, 167, 877-888. DOI:10.1144/0016-76492009-141

363 Callegaro, S., Baker, D.R., De Min, A., Marzoli, A., Geraki, K., Bertrand, H., Viti, C., Nestola, F.,
364 2014. Microanalyses link sulfur from large igneous provinces and Mesozoic mass extinctions.
365 *Geology*, 42, 895-898. DOI: 10.1130/G35983.1

366 Cirilli, S., 2010. Upper Triassic–Lowermost Jurassic Palynology and Palynostratigraphy: A
367 Review. In: Lucas, S.G., (Ed.), *The Triassic Timescale 334*. Geological Society, Special
368 Publications, London, pp. 285–314. DOI: 10.1144/SP334.12

369 Cirilli, S., Marzoli, A., Tanner, L., Bertrand, H., Buratti, N., Jourdan, F., Bellieni, G., Kontak, D.,
370 Renne, P.R., 2009. Latest Triassic onset of the Central Atlantic Magmatic Province (CAMP)
371 volcanism in the Fundy Basin (Nova Scotia): new stratigraphic constraints. *Earth and*
372 *Planetary Science Letters*, 286, 514–525. DOI: 10.1016/j.epsl.2009.07.021

373 Dal Corso, J., Marzoli, A., Tateo, F., Jenkyns, H.C., Bertrand, H., Youbi, N., Mahmoudi, A., Font,
374 E., Buratti, N., Cirilli, S., 2014. The dawn of CAMP volcanism and its bearing on the end-
375 Triassic carbon cycle disruption. *Journal of the Geological Society of London*, 171, 153-164.
376 DOI: 10.1144/jgs2013-063

377 Davies, J.H.F.L., Marzoli, A., Bertrand, H., Youbi, N., Ernesto, M., Schaltegger, U., 2017. End-
378 Triassic mass extinction started by intrusive CAMP activity. *Nature Communications*, 8, 1-8.
379 DOI: 10.1038/ncomms15596

380 Deenen, M.H.L., Ruhl, M., Bonis, N.R., Krijgsman, W., Kurschner, W.M., Reitsma, M., Van
381 Bergen, M.J., 2010. A new chronology for the end-Triassic mass extinction. *Earth and*
382 *Planetary Science Letters*, 291, 113–125. DOI: 10.1016/j.epsl.2010.01.003

383 Deenen, M.H.L., Krijgsman, W., Ruhl, M., 2011. The quest for chron E23r at Partridge Island, Bay
384 of Fundy, Canada: CAMP emplacement postdates the end-Triassic extinction event at the
385 North American craton. *Canadian Journal of Earth Sciences*, 48, 1282–1291. DOI:
386 10.1139/e11-015

387 Dickens, G.D., O'Neil, J., Rea, D.K., Owen, R.M., 1995. Dissociation of methane hydrate as a
388 cause of the carbon isotope excursion at the end of the Paleocene. *Paleoceanography*, 10,
389 965–971. DOI:10.1029/95PA02087.

390 El Hachimi, H., Youbi, N., Madeira, J., Bensalah, M.K., Martins, L., Mata, J., Medina, F., Bertrand,
391 H., Marzoli, A., Munhá, J., Bellieni, G., Mahmoudi, A., Abbou, M.B., Assafar, H., 2011.
392 Morphology, internal architecture and emplacement mechanisms of lava flows from the
393 Central Atlantic Magmatic Province (CAMP) of Argana Basin (Morocco). In: van
394 Hinsbergen, D.J.J., Buitter, S.J.H., Torsvik, T.H., Gaina, C., Webb, S.J. (Eds.), *The Formation
395 and Evolution of Africa: A Synopsis of 3.8 Ga of Earth History*. Geological Society, London,
396 Special Publications, 357, pp. 67–193. DOI: 10.1144/SP357.9

397 Fowell and Traverse, 1995. Late Triassic palynology of the Fundy basin, Nova Scotia and New
398 Brunswick. *Review of Palaeobotany and Palynology*, 86, 211–233.

399 Green, O.R., 2001. *A manual of practical laboratory and field techniques in palaeobiology*.
400 Dordrecht: Kuwer Academic Publishers. ISBN 0 412 58980 X.

401 Guex, J., Bartolini, A., Atudorei, V., Taylor, D., 2004. High-resolution ammonite and carbon
402 isotope stratigraphy across the Triassic-Jurassic boundary at New York Canyon (Nevada).
403 *Earth and Planetary Science Letters*, 225, 29–41. DOI: 10.1016/j.epsl.2004.06.006

404 Hesselbo, S.P., Robinson, S.A., Surlyk, F., Piasecki, S., 2002. Terrestrial and marine extinction at
405 the Triassic-Jurassic boundary synchronized with major carbon-cycle perturbation: A link to
406 initiation of massive volcanism?. *Geology*, 30, 251–254. DOI: 10.1130/0091-
407 613(2002)030<0251:TAMEAT>2.0.CO;2

408 Hesselbo, S.P., Robinson, S.A., Surlyk, F., 2004. Sea-level changes and facies development across
409 potential Triassic-Jurassic boundary horizons, SW Britain. *Journal of Geological Society of London*
410 161, 365–379. DOI: 10.1144/0016-764904-069.

411 Heunisch, C., Luppold, F.W., Reinhardt, L., Röhling, H.-G., 2010. Palynofazies, Bio-und
412 Lithostratigraphie im Grenzbereich Trias/Jura in der Bohrung Mariental 1 (Lappwaldmulde,

413 Ostniedersachsen). *Z. Dtsch. Ges. Geowiss.* 161, 51–98. DOI: 10.1127/1860- 804/2010/0161-
414 0051.

415 Hillebrandt, A.v., Krystyn, L., Kürschner, W.M., Bonis, N.R., Ruhl, M., Richoz, S., Schobben,
416 M.A.N., Urlichs, M., Bown, P.R., Kment, K., McRoberts, C.A., Simms, M., Tomášových, A.,
417 2013. The Global Stratotype Sections and Point (GSSP) for the base of the Jurassic System at
418 Kuhjoch (Karwendel Mountains, Northern Calcareous Alps, Tyrol, Austria). *Episodes*, 36,
419 162–198.

420 Irmis, R.B., Chure, D.J., Englemann, G.F., Wiersma, J.P., Lindström, S., 2015. The alluvial to
421 eolian transition of the Chinle and Nugget Formations in the southern Uinta Mountains,
422 northeastern Utah. In Vanden Berg, M.D., Resselar, R., Birgenheier, L.P., (Eds.). *The Uinta*
423 *Basin and Uinta Mountains: Utah Geological Association Publication 44*, 13- 48.

424 Knight, K.B., Nomade, S., Renne, P.R., Marzoli, A., Bertrand, H., Youbi, N., 2004. The Central
425 Atlantic Magmatic Province at the Triassic–Jurassic boundary: paleomagnetic and $^{40}\text{Ar}/^{39}\text{Ar}$
426 evidence from Morocco for brief, episodic volcanism. *Earth and Planetary Science Letters*,
427 228, 143–160. DOI: 10.1016/j.epsl.2004.09.022

428 Kürschner, W.M., Hengreen, G.F.W., 2010. Triassic palynology of central and northwestern
429 Europe: a review of palynofloral diversity patterns and biostratigraphic subdivisions.
430 Geological Society, London, Special Publications 334, 263-283. DOI: 10.1144/SP334.11

431 Kürschner, W.M., Bonis, N.R., Krystyn, L., 2007. Carbon-Isotope stratigraphy of the Triassic-
432 Jurassic transition in the Tiefengraben section, Northern Calcareous Alps. *Palaeogeography,*
433 *Palaeoclimatology, Palaeoecology*, 244, 257-280. DOI: j.palaeo.2006.06.031

434 Lindström, S., 2016. Palynofloral patterns of terrestrial ecosystem change during the end-Triassic
435 event – a review. *Geol. Mag.* 153, 223–251. DOI: 10.1017/S0016756815000552

436 Lindström, S., van de Schootbrugge, B., Dybkjær, K., Pedersen, G.K., Fiebig, J., Nielsen, L.H.,
437 Richoz, S., 2012. No causal link between terrestrial ecosystem change and methane release
438 during the end-Triassic mass-extinction. *Geology* 40, 531–534.

439 Lindström, S., Irmis, R.B., Whiteside, J.H., Smith, N.D., Nesbitt, S.J., Turner, A.H., 2016.
440 Palynology of the upper Chinle Formation in northern New Mexico, U.S.A.: Implications for
441 biostratigraphy and terrestrial ecosystem change during the Late Triassic (Norian–Rhaetian).
442 Review of Palaeobotany and Palynology 225, 106-131. DOI: 10.1016/j.revpalbo.2015.11.006

443 Lindström, S., van de Schootbrugge, B., Hansen, K.H., Pedersen, G.K., Alsen, P., Thibault, N.,
444 Dybkjær, K., Bjerrum, C.J., Nielsen, L.H., 2017. A new correlation of Triassic–Jurassic
445 boundary successions in NW Europe, Nevada and Peru, and the Central Atlantic Magmatic
446 Province: A time-line for the end-Triassic mass extinction. Palaeogeography,
447 Palaeoclimatology, Palaeoecology, 478, 80-102. DOI: 10.1016/j.palaeo.2016.12.025

448 Litwin, R.J., Traverse, A., Ash, S.R., 1991. Preliminary palynological zonation of the Chinle
449 Formation, southwestern U.S.A., and its correlation to the Newark Supergroup (eastern
450 U.S.A.). Review of Palaeobotany and Palynology 68, 269–287. DOI: 10.1016/0034-
451 667(91)90028-2.

452 Martindale, R.C., Berelson, W.M., Corsetti, F.A., Bottjer, D.J., West, A.J., 2012. Constraining
453 carbonate chemistry at a potential ocean acidification event (the Triassic–Jurassic boundary)
454 using the presence of corals and coral reefs in the fossil record. Palaeogeography,
455 Palaeoclimatology, Palaeoecology, 350–352, 114–123. DOI: 10.1016/j.palaeo.2012.06.020

456 Marzoli, A., Renne, P.R., Piccirillo, E.M., Ernesto, M., Bellieni, G., De Min, A., 1999. Extensive
457 200-million-year-old continental flood basalts of the Central Atlantic Magmatic Province.
458 Science, 284, 616–618. DOI: 10.1126/science.284.5414.616

459 Marzoli, A., Bertrand, H., Knight, K.B., Cirilli, S., Vérati, C., Nomade, S., Martini, R., Youbi, N.,
460 Allenbach, K., Neuwerth, R., Buratti, N., Rapaille, C., Zaninetti, L., Bellieni, G., Renne, P.R.,
461 2004. Synchrony of the Central Atlantic magmatic province and the Triassic–Jurassic
462 boundary climatic and biotic crisis. Geology, 32, 973-976. DOI: 10.1130/G20652.1

463 Marzoli, A., Jourdan, F., Puffer, J.H., Cuppone, T., Tanner, L.H., Weems, R.E., Bertrand, H.,
464 Cirilli, S., Bellieni, G., De Min, A., 2011. Timing and duration of the Central Atlantic

465 magmatic province in the Newark and Culpeper basins, eastern U.S.A. *Lithos*, 122, 175-188.
466 DOI: 10.1130/G20652.1

467 Marzoli, A., Davies, J.H.F.L., Youbi, N., Merle, R., Dal Corso, J., Dunkley, D.J., Fioretti, A.M.,
468 Bellieni, G., Medina, F., Wotzlaw, J.-F., McHone, G., Font, E., Bensalah, M.K., 2017.
469 Proterozoic to Mesozoic evolution of North-West Africa and Peri-Gondwana microplates:
470 Detrital zircon ages from Morocco and Canada. *Lithos*, 278-281, 229-239. DOI:
471 10.1016/j.lithos.2017.01.016

472 McElwain, J.C., Beerling, D.J., Woodward, F.I., 1999. Fossil plants and global warming at the
473 Triassic–Jurassic boundary. *Science*, 285, 1386–1390. DOI: 10.1126/science.285.5432.1386

474 Nomade, S., Knight, K.B., Beutel, E., Renne, P.R., Verati, C., Féraud, G., Marzoli, A., Youbi, N.,
475 Bertrand, H., 2007. Chronology of the Central Atlantic Magmatic Province: Implications for
476 the Central Atlantic rifting processes and the Triassic-Jurassic biotic crisis. *Palaeogeography,*
477 *Palaeoclimatology, Palaeoecology*, 344, 326-344. DOI: 10.1016/j.palaeo.2006.06.034

478 Percival, L.M.E., Ruhl, M., Hesselbo, S., Jenkyns, H., Mather, T.A., Whiteside, J., 2017. Mercury
479 evidence for pulsed volcanism during the end-Triassic mass extinction. *Proceedings of the*
480 *National Academy of Science*, 114, 7929–7934. DOI: 10.1073/pnas.1705378114

481 Raup, D.M., Sepkoski, J.J., 1982. Mass extinction in the marine fossil record. *Science* 215, 1501–
482 1502. DOI: 0036-8075/82/0319-1501\$01.00/0

483 Ruhl, M., Kürschner, W.M., 2011. Multiple phases of carbon cycle disturbance from large igneous
484 province formation at the Triassic–Jurassic transition. *Geology*, 39, 431–434. DOI:
485 10.1130/G31680.1

486 Ruhl, M., Kürschner, W.M., Krystyn, L., 2009. Triassic-Jurassic organic carbon isotope
487 stratigraphy of key sections in the western Tethys realm (Austria). *Earth and Planetary*
488 *Science Letters* 281, 169 - 187. DOI:10.1016/j.epsl.2009.02.020

489 Ruhl, M., Deenen, M.H.L., Abels, H.A., Bonis, N.R., Krijgsman, W., Kürschner, W.M. 2010.
490 Astronomical constraints on the duration of the early Jurassic Hettangian stage and recovery

491 rates following the end-Triassic mass extinction (St Audrie's Bay/East Quantoxhead, UK).
492 Earth and Planetary Science Letters, 295, 262–276. DOI: 10.1016/j.epsl.2010.04.008.

493 Ruhl, M., Bonis, N.R., Reichart, G-J, Sinninghe Damsté, J.S., Kürschner, W.M., 2011. Atmospheric
494 Carbon Injection Linked to End-Triassic Mass Extinction. *Science*, 333, 430-434.
495 DOI:10.1126/science.1204255

496 Schaller, M.F., Wright, J.D. & Kent, D.V., 2011. Atmospheric pCO₂ perturbations associated with
497 the Central Atlantic Magmatic Province. *Science*, 331, 1404–1409.
498 DOI:10.1126/science.1199011

499 Schoene, B., Guex, J., Bartolini, A., Schaltegger, U., Blackburn, T.J., 2010. Correlating the end-
500 Triassic mass extinction and flood basalt volcanism at the 100 ka level. *Geology*, 38, 387–
501 390. DOI:10.1130/G30683.1

502 Schnepf, E., Pucher, R., Goedicke, C., Manzano, A., Muller, U. & Lanos, P. (2003). Paleomagnetic
503 directions and thermoluminescence dating from a bread oven-floor sequence in Lqbeck
504 (Germany): a record of 450 years of geomagnetic secular variation. *Journal of Geophysical*
505 *Research* 108, 1-14. DOI:10.1029/2002JB001975

506 Svensen, H., Planke, S., Malthe-Sorensen, A., Jamtveit, B., Myklebust, R., Rasmussen Eidem, T.,
507 Rey, S.S., 2004. Release of methane from a volcanic basin as mechanism for initial Eocene
508 global warming. *Nature*, 429, 542–545. DOI: 10.1038/nature02566.

509 Thibodeau, A.M., Ritterbush, K., Yager, J.A., West, A.J., Ibarra, Y., Bottjer, D.J., Berelson, W.M.,
510 Bergquist, B.A., Corsetti, F.A., 106. The Mercury anomalies and the timing of biotic recovery
511 following the end-Triassic mass extinction. *Nature Communications* 7, 11147. DOI:
512 10.1038/ncomms11147

513 Verati, C., Rapaille, C., Féraud, G., Marzoli, A., Bertrand, H., Youbi, N., 2007. ⁴⁰Ar/³⁹Ar ages and
514 duration of the Central Atlantic Magmatic Province volcanism in Morocco and Portugal and
515 its relation to the Triassic-Jurassic boundary. *Palaeogeography, Palaeoclimatology,*
516 *Palaeoecology*, 244, 308-325. DOI:10.1016/j.palaeo.2006.06.033

517 Whiteside, J.H., Olsen, P.E., Eglinton, T., Brookfield M.E., Sambrotto, R.N., 2010. Compound-
518 specific carbon isotopes from Earth's largest flood basalt eruptions directly linked to the end-
519 Triassic mass extinction. PNAS.1001706107, 1-5. DOI:10.1073/pnas.1001706107

520 Wood, G.D., Gabriel, A.M., Lawson, J.C., 2002. Palynological Techniques-Processing and
521 Microscopy. In: Jansonius, J., McGregor, D.C. (Eds.), 2nd edition. Palynology: principles and
522 applications. American Association of Stratigraphic Palynologists Foundation 1, pp. 29–50.

523 Wotzlaw, J.-F., Guex, J., Bartolini, A., Gallet, Y., Krystyn, L., McRoberts, C.A., Taylor, D.,
524 Schoene, B., Schaltegger, U., 2014. Towards accurate numerical calibration of the late
525 Triassic: high-precision U-Pb geochronology constraints on the duration of the Rhaetian:
526 Geology, 42, 571–574. DOI: 10.1130/G35612.1

527 Yager, J.A., West, A.J., Corsetti, F.A., Berelson, W.M., Rollins, N.E., Rosas, S., Bottjer, D.J., 2017.
528 Duration of and decoupling between carbon isotope excursions during the end-Triassic mass
529 extinction and Central Atlantic Magmatic Province emplacement. Earth and Planetary Science
530 Letters, 473, 227-236. DOI: 10.1016/j.epsl.2017.05.031

531

532 **FIGURE CAPTIONS**

533 **Fig.1:** Location and geological setting of the study area. Schematic geology of the investigated
534 areas in the Argana Basin (Alemzi and Agouersuine sections), in Central High Atlas (southern
535 Tiourjdal section and northern Oued Lahr, Amassine and Ikourker sections), Middle Atlas (Ahouli
536 and Midelt, Tounfite and Agourai sections,) and Western Meseta region (Maaziz section).

537

538 **Fig.2:** Distributions of the recorded sporomorphs within the studied sections in Morocco. Below
539 Lower Basalt - Argana Basin, Alemzi and Agouersuine sections (samples AN101, AN131); central
540 High Atlas Basin: 1) South, Tiourjdal section (AN50, AN52, AN150); 2) North, Oued Lahr (AN59,
541 AN60) and Amassine (AN1) sections; Middle Atlas Basin, Midelt and Ahouli sections (AN214,
542 AN221) and Tounfite section (AN 533); Western Meseta region, Maaziz section (AN600). Below

543 Intermediate Basalt: Middle Atlas Basin, Agourai section (AN520). Above Upper Basalt: northern
544 central High Atlas Basin, Oued Lahr (AN69, AN203) and Ikourker (AN 64) sections.

545
546 **Fig. 3:** Sporomorphs from the studied sites in Morocco. A-E) Below Lower Basalt, southern central
547 High Atlas – Tiourjadal section; F) Below Lower Basalt, northern central High Atlas – Oued Lahr
548 section; G-H) Below Lower Basalt, Middle Atlas basin -Midelt and Ahouli sections; I) Below
549 Lower Basalt, Middle Atlas Basin – Tounfite section; J-K) Below Intermediate Basalt, Middle Atlas
550 basin – Agourai section; L) Above Upper Basalt, Central High Atlas Basin – Oued Lahr section. A)
551 *Patinasporites densus*, sample AN50, England Finder coordinates (E.F.c.) Q40(3); B) *Classopollis*
552 *meyerianus*, AN50 E.F.c. C36(3); C) *Classopollis murphyae*, AN50 E.F.c. C29(1); D) *Classopollis*
553 *murphyae*, AN50 E.F.c. L30(1); E) *Vitreisporites pallidus*, AN52 E.F.c. O49(1); F) *Classopollis*
554 *torosus*, AN59 E.F.c. J44(2); G) *Patinasporites densus*, AN214 E.F.c. E40(2); H) *Ovalipollis* sp.,
555 AN214 E.F.c. E36(2); I) *Ovalipollis pseudoalatus*, AN533 E.F.c. D41(3); J) *Patinasporites densus*,
556 AN520 E.F.c. K31(3); K) *Tsugaepollenites pseudomassulae*, AN520 E.F.c. H53(1); L)
557 *Patinasporites densus*, AN64, E.F.c. T19(3). Scale Bar 10 µm.

558
559 **Fig. 4:** An attempt to correlate the Tiourjadal section (CHA, Morocco) with the GSSP section for the
560 Tr-J boundary (Khujoch, Austria) (Hillebrandt et al., 2013) and with St. Audrie's Bay (UK) section
561 (Bonis et al., 2010), based on palynological associations, ammonites, $\delta^{13}\text{C}$ -isotopes,
562 geochronological data (Blackburn et al., 2013) and Hg/TOC (Percival et al., 2017). Geochemical
563 data of Morocco section are from Dal Corso et al., 2014). The negative carbon isotope shift at the
564 base of the Lower Basalt can be referred to the *initial* CIE, according to the traditional correlation
565 by (Hesselbo et al., 2002, 2004; Ruhl et al., 2010; Hillebrandt et al., 2013) (red dotted line labelled
566 as 1), and to the *Marshi* CIE, according to Lindström et al. (2017) (red dotted line labelled as 2).
567 Beyond the possible correlations that can be adopted, the new palynological data discussed in this

568 study indicate a Rhaetian age for the most part of the sedimentary strata intercalated with the
569 CAMP basalts, thus excluding an Early Jurassic age for the volcanic pile.

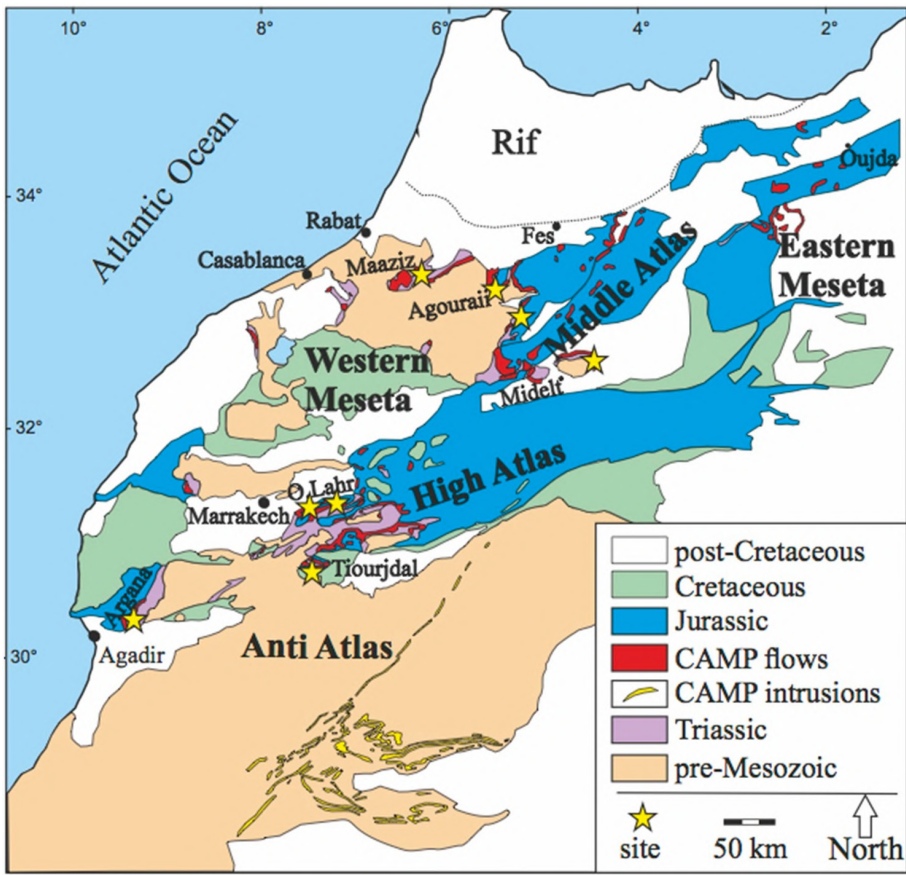


Fig 1

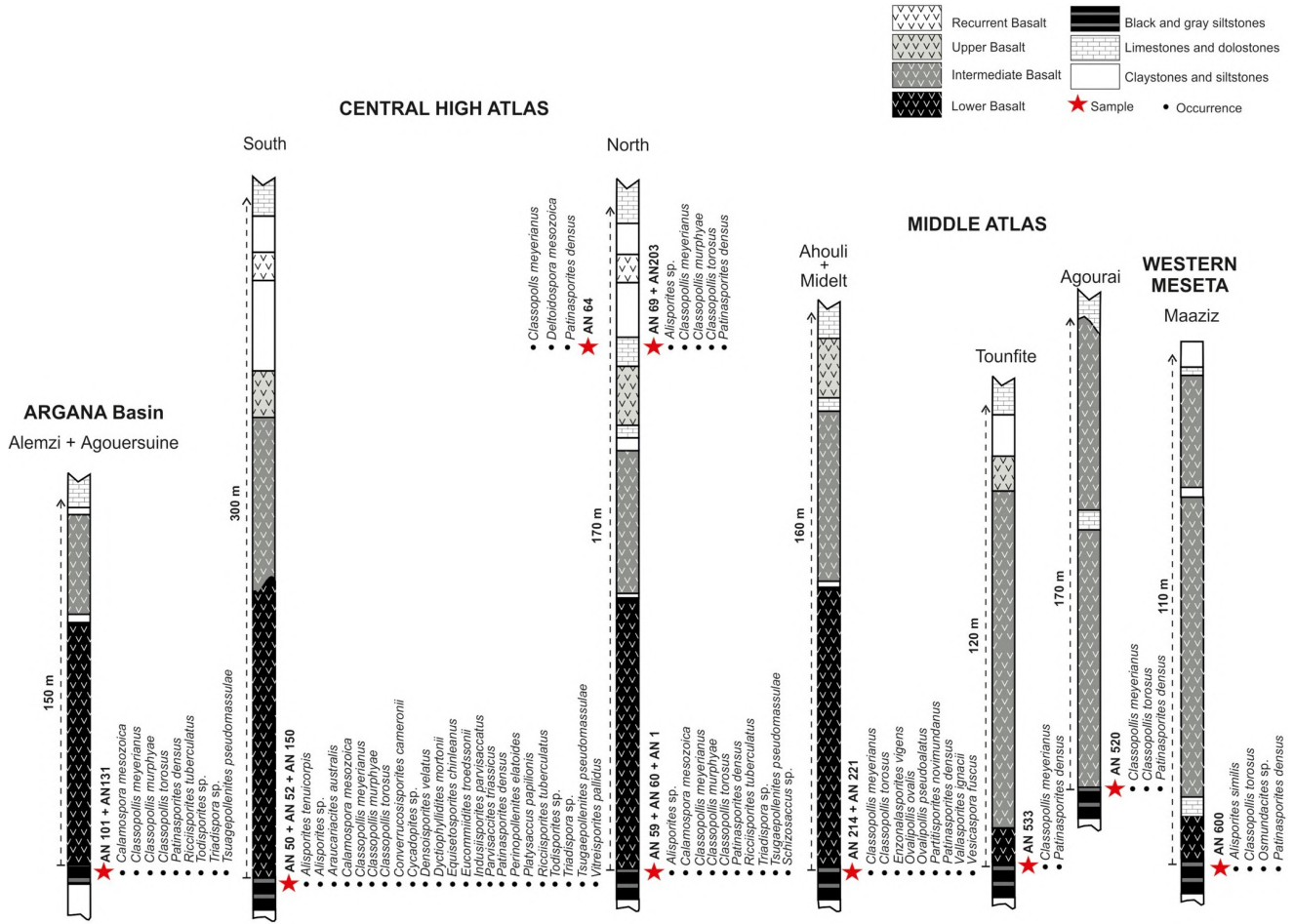


Fig. 2.

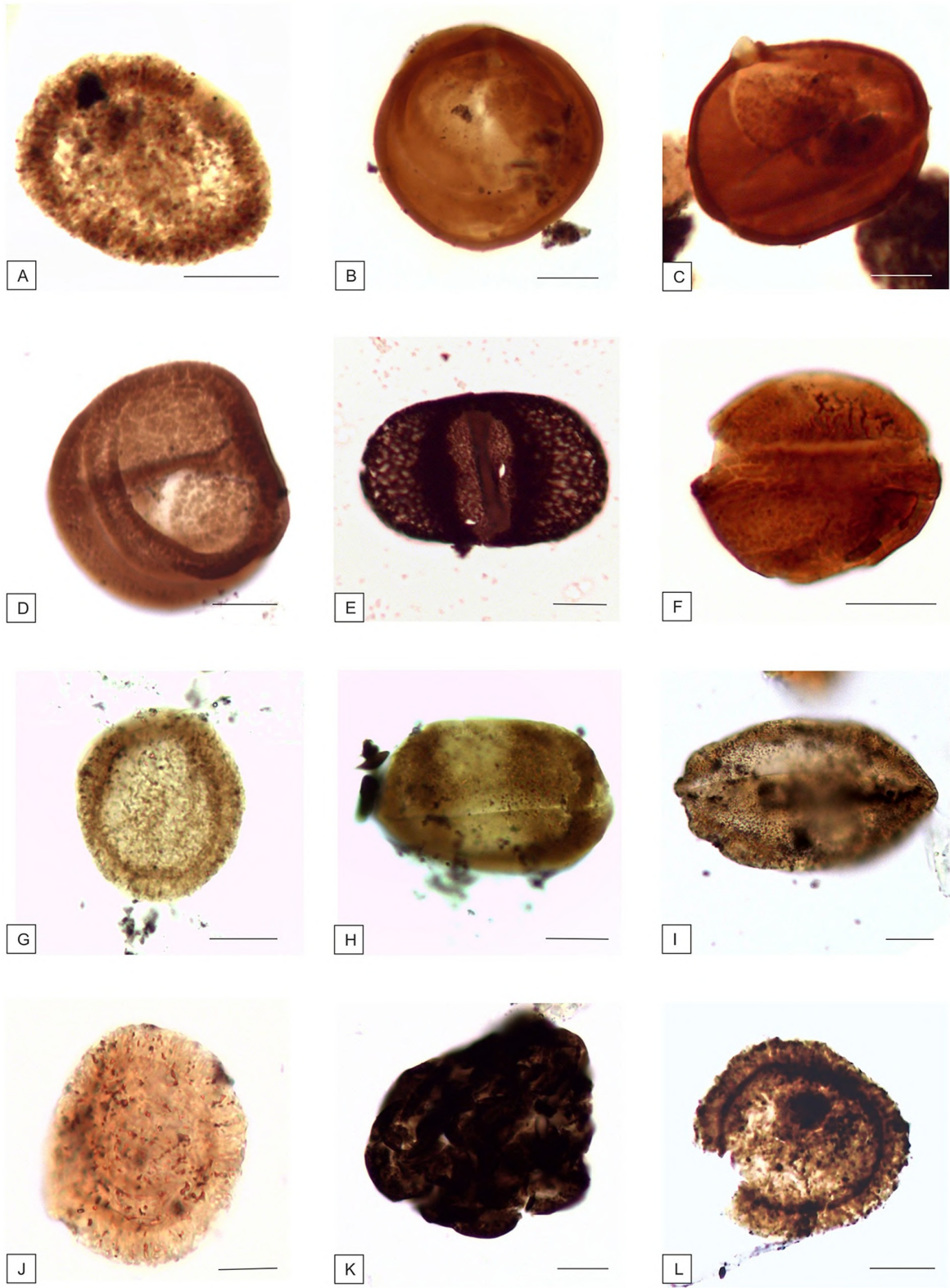


Fig. 3.

Kuhjoch (Austria)

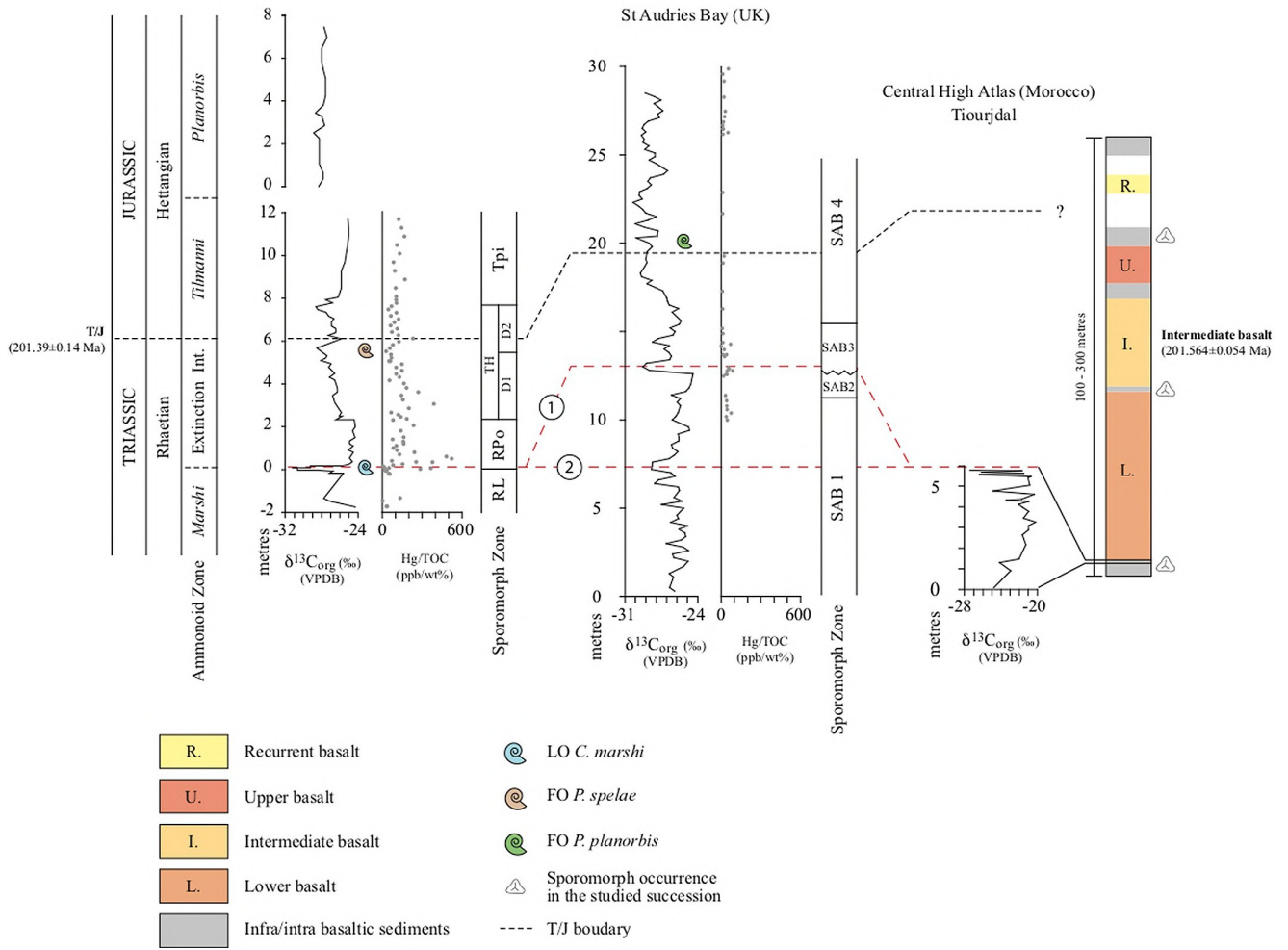


Fig. 4.